Hypomorphic Notch 3 alleles link Notch signaling to ischemic cerebral small-vessel disease

Joseph F. Arboleda-Velasquez[a], Jan Manent[a], Jeong Hyun Lee[b], Saara Tikka[a,c], Carolina Ospina[a,d], Charles R. Vanderburg[e], Matthew P. Frosch[e,f], Manuel Rodríguez-Falcón[g], Judit Villen[a,1], Steven Gygi[a], Francisco Lopera[h], Hannu Kalimo[c], Michael A. Moskowitz[b], Cenk Ayata[b], Angeliki Louvi[d,2], and Spyros Artavanis-Tsakonas[a,i,2]

[a]Department of Cell Biology, Harvard Medical School, Boston, MA 02115; [b]Departments of Radiology and Neurology, Stroke and Neurovascular Regulation Laboratory, Massachusetts General Hospital and Harvard Medical School, Charlestown, MA 02129; [c]Protein Chemistry Unit, Institute of Biomedicine/Anatomy and Haartman Institute, Department of Pathology, University of Helsinki, 00014 Helsinki, Finland; [d]Program on Neurogenetics and Departments of Neurosurgery and Neurobiology, Yale School of Medicine, New Haven, CT 06520; [e]Harvard NeuroDiscovery Center, Boston, MA 02129; [f]Alzheimer Research Unit, Mass General Institute for Neurodegenerative Disease, Department of Neurology and C.S. Kubik Laboratory for Neuropathology, Pathology Service, Massachusetts General Hospital and Harvard Medical School, Boston, MA 02114; [g]Proteomics Unit, Department of Experimental and Health Sciences, Pompeu Fabra University, 08003 Barcelona, Spain; [h]Grupo de Neurociencias de Antioquia, Universidad de Antioquia, AA 1226 Medellín, Colombia; and [i]Collège de France, 75005 Paris, France

Edited* by Pietro De Camilli, Yale University and The Howard Hughes Medical Institute, New Haven, CT, and approved April 14, 2011 (received for review February 4, 2011)

The most common monogenic cause of small-vessel disease leading to ischemic stroke and vascular dementia is the neurodegenerative syndrome cerebral autosomal-dominant arteriopathy with subcortical infarcts and leukoencephalopathy (CADASIL), which is associated with mutations in the Notch 3 receptor. CADASIL pathology is characterized by vascular smooth muscle cell degeneration and accumulation of diagnostic granular osmiophilic material (GOM) in vessels. The functional nature of the Notch 3 mutations causing CADASIL and their mechanistic connection to small-vessel disease and GOM accumulation remain enigmatic. To gain insight into how Notch 3 function is linked to CADASIL pathophysiology, we studied two phenotypically distinct mutations, C455R and R1031C, respectively associated with early and late onset of stroke, by using hemodynamic analyses in transgenic mouse models, receptor activity assays in cell culture, and proteomic examination of postmortem human tissue. We demonstrate that the C455R and R1031C mutations define different hypomorphic activity states of Notch 3, a property linked to ischemic stroke susceptibility in mouse models we generated. Importantly, these mice develop osmiophilic deposits and other age-dependent phenotypes that parallel remarkably the human condition. Proteomic analysis of human brain vessels, carrying the same CADASIL mutations, identified clusterin and collagen 18 α1/endostatin as GOM components. Our findings link loss of Notch signaling with ischemic cerebral small-vessel disease, a prevalent human condition. We determine that CADASIL pathophysiology is associated with hypomorphic Notch 3 function in vascular smooth muscle cells and implicate the accumulation of clusterin and collagen 18 α1/endostatin in brain vessel pathology.

Ischemic cerebral small-vessel disease is increasingly recognized as a prevalent cause of ischemic stroke and vascular cognitive impairment (1). In most cases, ischemic cerebral small-vessel disease is associated with cardiovascular risk factors and old age (1), although Mendelian forms resembling key aspects of the pathophysiology of the disease, in the absence of cardiovascular risk factors, have been identified (2–5). The most common familial form of ischemic cerebral small-vessel disease is defined by cerebral autosomal-dominant arteriopathy with subcortical infarcts and leukoencephalopathy (CADASIL), an inherited, dominant, late-onset syndrome that has been associated with mutations in *NOTCH 3* (2), encoding one of the four vertebrate Notch receptor paralogues. Patients with CADASIL develop widespread arteriopathy that manifests itself most severely in brain vessels, eventually causing chronic ischemic degeneration of neurons and glia (2, 6–12). CADASIL brain pathology reveals severe leukoencephalopathy, vascular smooth muscle cell (vSMC) degeneration, and the appearance of pathognomonic granular osmiophilic deposits, termed granular osmiophilic material (GOM), of unknown composition (9, 10). In adult tissues, Notch 3 expression is restricted to arterial vSMC, which are also the focus of CADASIL pathology (13). Studies in knockout mouse models implicated Notch 3 activity in vSMC differentiation (14, 15) and in the susceptibility of the brain to ischemic challenges (16). However, the role of Notch signaling in CADASIL pathobiology, the nature of the CADASIL mutations, and the mechanisms associating Notch 3 activity to vessel degeneration, remain enigmatic (8, 13).

The Notch receptor is the central element of a fundamental cell interaction mechanism that links the fate choice of one cell to that of its cellular neighbors (17, 18). Aberrant Notch signaling in humans has been associated with diverse pathogenic conditions, including developmental syndromes and cancer (13). The Notch receptors are single-pass transmembrane proteins with a large extracellular domain that contains, depending on the paralogue, 30 to 36 EGF-like repeats. The extracellular domain interacts with the membrane-bound ligands Delta or Serrate/Jagged (13) expressed on the surface of juxtaposed cells, triggering a proteolytic cascade that releases the intracellular domain of Notch, allowing it to translocate into the nucleus, where it directs target gene transcription (18).

CADASIL mutations typically affect single extracellular cysteine residues in individual EGF-like repeats resulting in mutant receptors of unknown functionality (2, 8, 13, 19). We focus here on two mutations associated with strikingly different clinical phenotypes, based on detailed clinical assessments (20). The C455R mutation results in a distinct, and apparently more severe, phenotype with the median age at onset of stroke preceding by more than two decades that of individuals carrying the R1031C mutation. The early-onset phenotype is accompanied by extensive white-matter abnormalities identified by MRI (20). We generated transgenic mouse models to examine the biology and functionality of these mutations, and analyzed postmortem hu-

Author contributions: J.F.A.-V., J.M., A.L., and S.A.-T. designed research; J.F.A.-V., J.M., J.H.L., S.T., C.O., M.R.-F., J.V., and A.L. performed research; C.R.V., S.G., and F.L. contributed new reagents/analytic tools; J.F.A.-V., J.M., S.T., M.P.F., S.G., H.K., M.A.M., C.A., A.L., and S.A.-T. analyzed data; and J.F.A.-V., A.L., and S.A.-T. wrote the paper.

The authors declare no conflict of interest.

*This Direct Submission article had a prearranged editor.

[1]Present address: Department of Genome Sciences, University of Washington, Seattle, WA 98195.

[2]To whom correspondence may be addressed. E-mail: angeliki.louvi@yale.edu or artavanis@hms.harvard.edu.

See Author Summary on page 8537.

This article contains supporting information online at www.pnas.org/lookup/suppl/doi:10.1073/pnas.1101964108/-/DCSupplemental.

man tissue of patients carrying identical mutations. The transgenic models show striking parallels with the human disease including the development of osmiophilic deposits and the age-dependent appearance of mutant phenotypes.

Results

CADASIL Mutations Reflect Hypomorphic Activity of Notch 3 in Vivo. To explore the functionality of CADASIL mutations, we chose to focus on two mutations, which display significantly diverse phenotypes in terms of clinical severity in Colombian families with the disease, allowing us therefore to gain insights into genotype–phenotype relationships. The C455R mutation maps within the 11th EGF-like repeat, a region associated with ligand binding, whereas the R1031C mutation affects the 26th EGF-like repeat (20, 21). To evaluate the relative activity of each mutant receptor, we generated conditional mouse strains that harbored *NOTCH 3* transgenes encoding the WT (16) or each of the two mutant receptors from the ROSA26 locus to ensure their expression at similar levels, a prerequisite for comparative studies given the sensitivity of development to Notch dosage (13) (Fig. 1*A* and *B*).

Given that *Notch 3* KO mice have been shown to be strikingly susceptible to ischemic brain injury, a phenotype that can be rescued by expressing WT *NOTCH 3* in vSMCs, we measured Notch receptor activity by using this assay (16). We thus examined the ability of the CADASIL *NOTCH 3* transgenes to rescue the ischemia susceptibility phenotype of *Notch 3* KO mice when expressed in vSMC. Receptor activity was evaluated through standard filament occlusion of the middle cerebral artery (MCA), followed by measurements of the stroke area 24 h after reperfusion, as described before (16) (Fig. 1*C*). As expected, SM22-Cre mediated expression of *NOTCH 3*^{WT} in vSMCs reduced infarct volume in 3-mo-old *Notch 3* KO animals, effectively rescuing the stroke susceptibility phenotype (Fig. 1*C*). Expression of the *NOTCH 3*^{R1031C} transgene also rescued stroke susceptibility (Fig. 1*C*). In contrast, expression of the *NOTCH 3*^{C455R} transgene failed to rescue the phenotype (Fig. 1*C*). Thus, the C455R mutation, which in humans is associated with an early onset of stroke (20), likely reflects a loss-of-function allele.

The fact, however, that the R1031C mutation rescues the stroke susceptibility phenotype as efficiently as the WT does not demand that the R1031C receptor has WT activity. The ROSA26 driven overexpression of a weak hypomorphic mutation may still be capable to provide enough activity to rescue the KO phenotype. Given the degenerative nature of CADASIL, we reasoned that the ability of the R1031C mutant receptor to rescue the stroke susceptibility phenotype in 3- to 6-mo-old *Notch 3* KO animals (Fig. 1*C*) may be age-dependent, if indeed this allele is a weak hypomorph, and thus challenged 1-y-old mice using the same experimental paradigm. Indeed, at this older age, expression of the R1031C mutant receptor failed to rescue the stroke susceptibility phenotype of the *Notch 3* KO animals (Fig. 1*D*). This parallels the progressive nature of CADASIL pathology in humans and the late onset of stroke associated with the R1031C mutation in the Colombian kindred. Thus, it is likely that both Colombian CADASIL mutations reflect distinct hypomorphic states of the Notch 3 receptor.

CADASIL Mutations Reflect Hypomorphic Activity of Notch 3 in Vitro. Previous analyses of CADASIL mutations, albeit different from those examined here, favored the notion that they reflect neo-

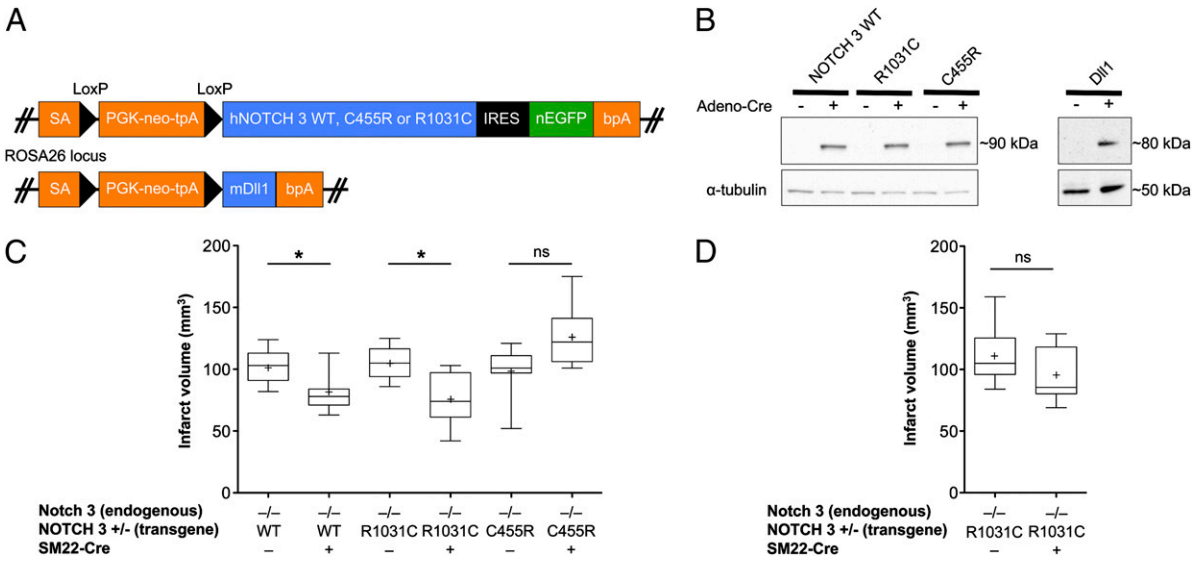

Fig. 1. CADASIL mutations in Notch 3 reflect hypomorphic receptor activity in vivo. (*A*) Transgenic mouse models for in vivo studies of Notch signaling. Schematic representation of the targeting vectors used to generate conditional knock-in mice expressing human Notch 3 WT (hNOTCH3 WT), or the C455R or R1031C mutant receptors, or the mouse Dll1 ligand (also see ref. 16). Each construct contains genomic sequences allowing for homologous recombination into the ROSA locus; an adenovirus splice acceptor (SA); a PGK-neo-tpA "stop" cassette flanked by loxP sites (black triangles) allowing for Cre-mediated excision; the transgene; and the bovine growth hormone polyadenylation sequence (bpA). The *NOTCH 3* WT and mutant transgenes are followed by an internal ribosomal entry site (IRES) and nuclear EGFP (nEGFP). (*B*) Western blot analysis of protein cell lysates shows conditional expression of Notch 3 receptors (S1-cleaved N fragment containing the transmembrane and intracellular domains, ~90 kDa, in aorta-derived SMC cultures) and of Dll1 ligand (~80 KDa, in MEFs), upon infection with adeno-Cre. The Notch 3 WT and mutant receptors are expressed at similar levels allowing for comparative studies. (*C* and *D*) Functional analysis of receptor activity in vivo presented as box-and-whisker plots. Cerebral infarcts were produced by MCA occlusion (1 h) followed by reperfusion in adult *Notch 3* KO male mice expressing the different *NOTCH 3* transgenes as indicated. Infarct volumes are calculated by integrating the infarct area in each brain section, using the indirect method to correct for edema (*Methods*). (*C*) In 3- to 6-mo-old mice, expression of WT or R1031C mutant receptors in vSMCs, using the SM22-Cre driver, rescues the ischemia susceptibility phenotype of *Notch 3* KO animals, whereas expression of C455R mutant receptors does not. (*D*) In 1-y-old mice, expression of R1031C mutant receptors in vSMCs no longer rescues the ischemia susceptibility phenotype. The line bisecting the box in the plot is the median value, the cross is the mean, the upper and lower limits of the box are the 25th and 75th percentile values; the whiskers extend to the lowest and highest values. At least five animals were analyzed in each experimental group (*Methods*).

morphic mutants mainly based on the lack of convincing evidence that Notch 3 receptors carrying CADASIL mutations can be associated with impaired signaling (14, 21–25). To obtain additional evidence for the functionality of the two CADASIL mutations under study, independently of the aforementioned physiologic assays, we sought to directly measure the ability of the receptors to signal using a cell-based assay. The available ligand-dependent assays for measuring the ability of Notch receptors to drive the transcription of a reporter do not offer the necessary sensitivity to reliably evaluate differences associated with different hypomorphic mutations, and thus we attempted to develop a more suitable assay. For this, we isolated primary mouse embryonic fibroblasts (MEFs) from our conditional mice carrying the WT or mutant Notch 3 receptor transgenes in a *Notch 3* KO background and from a conditional transgenic mouse conditionally expressing the Notch ligand Delta-like 1 (Dll1) (26) (Fig. 1*A*).

To induce expression of the transgenes encoding the Dll1 ligand and the Notch 3 receptors, MEFs were infected with an adenovirus encoding the Cre recombinase (adeno-Cre) 24 h before coculture. MEFs expressing the ligand and WT or mutant Notch 3 receptors were subsequently cocultured (Fig. 2*A*), and after 48 h, the receptor-expressing cells were isolated by using FACS by virtue of their also expressing EGFP (Fig. 1*A* and Fig. 2*A*). Having established, through quantitative PCR (qPCR), that *Heyl* and *Hey1* are both targets of ligand-dependent Notch signaling in MEFs, we based the evaluation of Notch 3 receptor activity on comparing the levels of *Heyl* and *Hey1* transcripts by using qPCR (Fig. 2 *B* and *C*). When we compared Notch activity of homozygous or heterozygous combinations of the Notch 3 alleles at hand, we determined that the highest activity levels were associated with MEFs of the R1031C/WT genotype, followed by R1031C/R1031C homozygotes, C455R/WT, and finally with the C455R/C455R homozygotes displaying the lowest activity. This allelic series corroborates the notion that the CADASIL mutations we examine are hypomorphs, with the R1031C mutation defining a weaker loss of function allele than C455R. We note that the genotype–phenotype correlations we define through our mouse models parallels those observed in individuals carrying the same mutations.

CADASIL Transgenic Mice Develop Electron-Dense Granular Deposits and vSMC Abnormalities. The analysis of the CADASIL mouse models was extended by exploring the pathognomonic phenomenon associated with the disease in humans, namely GOM accumulation in the vasculature (10, 12, 27, 28). Both the composition as well as the possible functional consequences of these deposits are unknown (13). Nevertheless, we were encouraged to examine this phenomenon by the reported findings that mice overexpressing Notch 3 receptors carrying different CADASIL mutations develop what are suggested to be deposits analogous to human GOMs in the vasculature (24, 29, 30).

Animals expressing the R1031C mutant Notch 3 receptor in vSMCs showed osmiophilic granular deposits in brain vessels even though they carry a WT endogenous *Notch 3* allele as in the human condition; however, these deposits were evident only in animals older than 12 mo (Fig. 3 *A–D*) and not in 6-mo-old animals. These animals also developed vSMC abnormalities with intracellular inclusions and lipid droplets that were more severe in older mice (age 19–20 mo) with the R1031C mutation compared with younger R1031C carriers or to mice expressing *NOTCH 3*^{WT} (Fig. 3). Whereas a similar aging study remains to be completed with the C455R mutation, we do note that mice carrying the C455R mutation in a *Notch 3* KO background—the genotype analyzed in our hemodynamic studies (Fig. 1)—showed electron-dense deposits and vSMC abnormalities at a much younger age (6 mo; Fig. 3 *E* and *F*).

The definition of GOMs derives from CADASIL patient tissue, relying on purely morphological criteria. Thus, it is essential to emphasize that we cannot rigorously conclude that the deposits we see in mice are indeed identical to GOMs. In individuals with CADASIL, GOMs are essentially found in the extracellular milieu and in close association with the plasma membrane of vSMCs (11), whereas in our mice, at least at the stages examined, some osmiophilic deposits appear to be intracellular, associated with vesicles and inclusions. Notwithstanding such differences, the age-dependent appearance of the deposits in vSMCs correlates with the expression of Notch 3 receptors carrying CADASIL mutations, and is consistent with the notion that the deposits in mice and the human GOMs reflect analogous phenomenology. More-

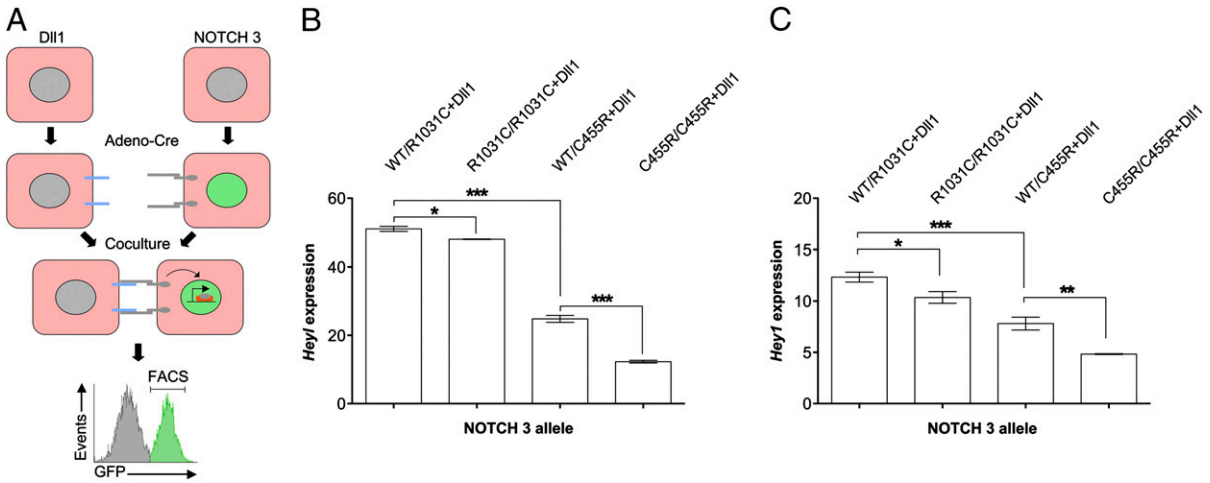

Fig. 2. CADASIL mutations reflect hypomorphic Notch 3 receptor activity in vitro. (*A*) Schematic of the ligand-dependent Notch receptor activity coculture assay. MEFs isolated from mice were induced to express Notch 3 WT or mutant receptors or the Dll1 ligand using adeno-Cre infection and then cocultured for 48 h. Receptor-expressing cells were isolated by FACS. (*B* and *C*) Expression of *Heyl* (*B*) and *Hey1* (*C*) in receptor-expressing cells assessed by qPCR. MEFs carrying two copies of the transgenes in homozygous (R1031C/R1031C and C455R/C455R) or heterozygous (WT/R1031C and WT/C455R) combinations were analyzed. The expression of *Heyl* and *Hey1* was significantly lower in MEFs expressing homozygous combinations of the CADASIL alleles than their heterozygous counterparts. These results define an allelic series with the C455R mutation representing the stronger loss-of-Notch-function allele. Error bars indicate SDs. Data are representative of three independent experiments. Note that the activation of *Heyl* expression in this Notch signaling assay is far more robust than that of *Hey1* across experiments. Statistically significant differences: $*P < 0.05$, $**P < 0.01$, and $***P < 0.005$.

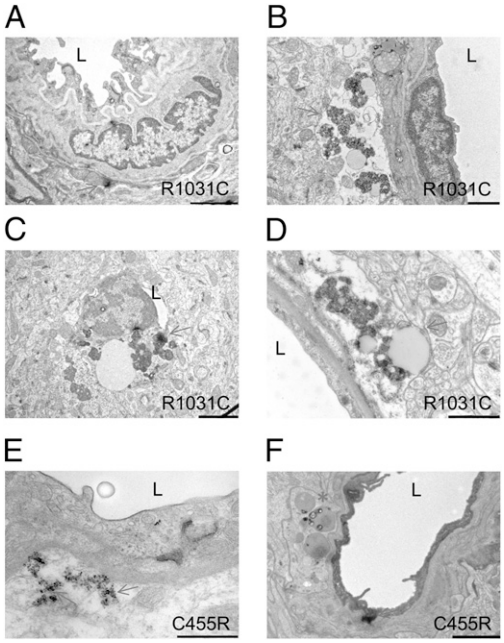

Fig. 3. CADASIL transgenic mice develop vSMC abnormalities. (*A–D*) Representative electron micrographs from 12- to 14-mo-old (*A–C*) ($n = 2$) or 19- to 21-mo-old (*D*) ($n = 2$) animals carrying the human R1031C mutation in a mouse *Notch 3* WT background. Morphological abnormalities were absent in animals carrying the R1031C mutation at 6 mo of age ($n = 2$). (*E* and *F*) Representative EM images from 6-mo-old animals carrying the C455R mutation in a *Notch 3* KO background ($n = 2$). (*A*) Overview of a vessel with abundant elastin and an electron-dense granular deposit (arrow). (*B*) Accumulation of extracellular granular material (arrow) and cytoplasmic inclusions (asterisk). (*C*) An almost occluded vessel with accumulations of granular material. (*D*) Accumulation of granular material and inclusions (arrow). (*E*) Accumulation of electron-dense granular material (arrows). (*F*) Inclusions (asterisk) and electron-dense granular material (arrow). The brain tissue analyzed was compared with tissue from age-matched controls expressing the WT *NOTCH* 3 ($n = 5$) and from animals that lacked the SM22-Cre driver ($n = 5$) processed in parallel. L, lumen. (Scale bars: *A*, 2 μm; *B* and *C*, 1 μm; *D* and *F*, 2 μm; *E*, 500 nm.)

over, these observations raise the intriguing possibility that, in the model system, we may be witnessing the biogenesis of GOMs.

Analyses of GOM Deposits in CADASIL Postmortem Brain. Despite the pathognomonic nature of GOMs in the diagnosis of CADASIL, their composition remains unknown. The availability of postmortem brain tissue from patients with CADASIL carrying the R1031C mutation allowed us to attempt a proteomics approach to address this important issue. Tunica media was targeted in brain arteries by laser capture microdissection (LCM) and subsequently analyzed by MS (*Methods*). Approximately 1,200 arterial rings were collected from two brains from individuals with CADASIL and two sex- and age-matched control subjects without clinical history or brain pathology. Within the list of approximately 1,000 proteins identified in each sample by MS, proteins classified by gene ontology under "muscle contraction" and "muscle development" were enriched ($P < 0.05$) in both CADASIL and control samples, validating the correct tissue targeting of the LCM (Tables S1 and S2).

Comparative proteome profiling analysis (*Methods*) identified 19 proteins that were differentially expressed in CADASIL versus control samples (Table S3). We focused on two of these proteins on the basis of their described functionalities, collagen 18 α1 (COL18A1) and clusterin. Both were more prevalent in CADASIL samples. COL18A1 is cleaved posttranslationally to give rise to endostatin, a C-terminal proteolytic fragment with strong antiangiogenic properties (31, 32), whereas clusterin functions as an extracellular chaperone (33). Interestingly, *CLUSTERIN* variants have been associated with Alzheimer disease in humans (34–36) and the protein has been associated with extracellular deposits in several disorders (37). It is noteworthy that our proteomic analysis did not identify Notch 3 itself as a component of the protein extracts analyzed, notwithstanding suggestions that Notch 3 extracellular antigens are found in association with, or within, GOMs, albeit in brains of patients carrying different CADASIL mutations (27, 38). The reason for this apparent incongruity remains to be established, and it may reflect the fact that we are analyzing different CADASIL mutations and/or the different analytical approaches used.

To determine the relationship of these two proteins with the GOMs, we examined postmortem brain tissue from patients with CADASIL by immunocytochemistry using available antibodies (Figs. 4 and 5). Given that most COL18A1 peptides identified by MS derive from the C-terminal of the protein (Fig. 5*A*), we used endostatin-specific antibodies for our analysis (Fig. 5). We examined postmortem tissue derived from R1031C carriers, the source for the proteomic analysis, from individuals carrying the C455R, G528C, and Y1069C mutations, as well as tissue from nine individuals with the R133C mutation, which is prevalent in Scandinavian populations (39). All samples confirmed an abnormal vascular distribution for clusterin and COL18A1/endostatin (Figs. 4 and 5) in brain vessels. Both appeared abundant in the media of CADASIL-affected vessels, a distribution resembling that of GOMs and of periodic acid–Schiff (PAS)–positive deposits (Figs. 4 and 5), which abound at the innermost region of the tunica media in CADASIL (11). We note that clusterin staining was stronger in white rather than gray matter arteries (Fig. 4 *E–H*), consistent with the known association of CADASIL pathology with subcortical vessels (9, 12, 40, 41). To examine if clusterin and COL18A1/endostatin were indeed enriched in GOMs, which are defined through EM, we examined the distribution of these proteins by immuno-EM on brain tissue from individuals carrying the C455R or R1031C mutations. Both proteins could be identified within the GOMs (Figs. 4 *K* and *L* and 5*G*), raising the possibility that abnormal distribution and accumulation of clusterin and COL18A1/endostatin may carry diagnostic value.

Functional Links Among Notch, Clusterin, and COL18A1/Endostatin. Although a functional link among *NOTCH 3* mutations, CADASIL vessel pathology, and either COL18A1/endostatin or clusterin remains to be established, we explored the mouse model under the presumption that biologically important links will be conserved across species barriers.

To probe if the expression of Notch 3 mutant receptors had impact on clusterin and COL18A1/endostatin, we used the aorta, a tissue that is more accessible than brain vasculature for biochemical studies. EM analyses of aortas from mice expressing the R1031C mutation consistently showed overt abnormalities, including thinning of the vSMC layers, reminiscent of the arteriopathy observed in patients with CADASIL (9, 12, 40, 41) (Fig. 6*A* and *B*). Hence, animals carrying the R1031C mutation, in addition to the mutant phenotypes described earlier, also show a Notch-dependent morphological phenotype in the aorta. Immunoblot analysis demonstrated that both clusterin and COL18A1/endostatin showed significant accumulation in aortas from 18-mo-old mice expressing the R1031C mutation compared with analogous tissue from animals expressing WT Notch 3 (Fig. 6*C*). This parallels our observations in humans, strengthening the notion of a functional link between Notch 3 activity and the two proteins identified by proteomics analysis of diseased vessels, clusterin and COL18A1/endostatin.

Discussion

The present study indicates that the two CADASIL mutations we examined, C455R and R1031C, reflect hypomorphic Notch 3

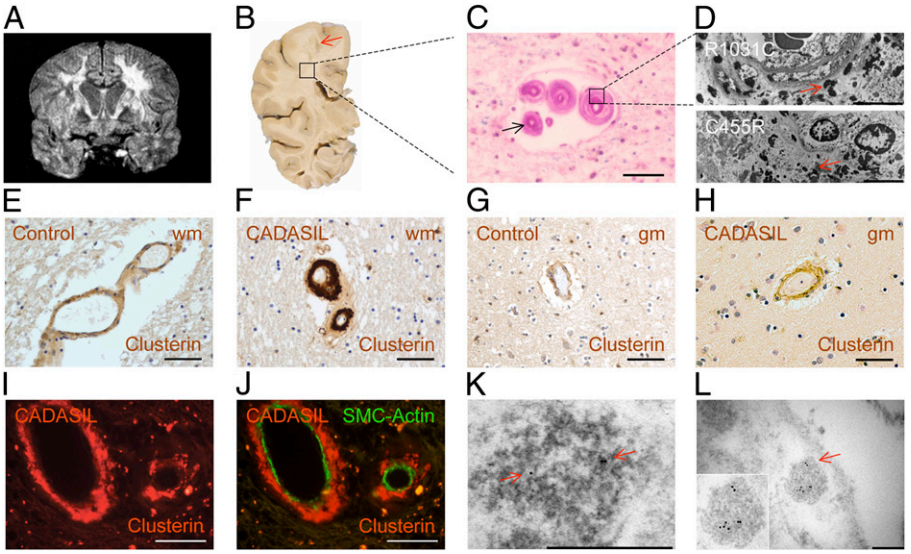

Fig. 4. Molecular characterization of postmortem cerebral vessels from individuals with CADASIL. (*A*) Coronal MRI of the proband individual of the Colombian kindred with CADASIL carrying the R1031C mutation shows extensive bilateral leukoencephalopathy. (*B*) Photograph of postmortem coronal section of the left cerebral hemisphere at the level of the lateral geniculate nucleus shows loss of white matter, evident in the centrum semiovale (arrow). (*C*) Photomicrograph of deep subcortical white matter stained with Luxol fast blue (LFB)/PAS) shows marked hyalinization of the vessel walls, rare myelin sheaths (in blue), and PAS-positive deposits (arrow). (*D*) EM images of subcortical white matter of postmortem brains from individuals carrying the R1031C (*Upper*) and C455R (*Lower*) mutations show abundant electron-dense GOM deposits. (*E–H*) Immunohistochemical staining shows abnormal accumulation of clusterin in brains from individuals carrying the R133C mutation (*F* and *H*) compared with age-matched controls (*E–G*). Consistent with the severity of vessel pathology, clusterin staining is stronger in white matter (wm) than in gray matter (gm) arteries. (*I* and *J*) Clusterin is localized to the tunica media of the arteries but is excluded from the few remaining smooth muscle cells, labeled with α-actin (SMC-actin), in tissue from an individual with the R133C mutation. (*K* and *L*) Brain tissue from an individual with the C455R mutation was processed for immunogold labeling with an antibody against clusterin, which is detected in GOMs. (Scale bars: *C* and *E–I*, 50 μm; *D*, 5 μm; *K*, 500 nm; *L*, 200 nm.)

receptor function. Information regarding the functionality of the receptor is an essential prerequisite for any rational therapeutic approach, and, although it is reasonable, on the basis of our analysis, to hypothesize that all CADASIL mutations reflect hypomorphic Notch 3 activity, additional functional studies are essential to reach a general conclusion. If indeed all CADASIL mutations reflect loss of Notch function, the dominant nature of CADASIL could be attributed to dosage effects—which is quite conceivable given that haploinsufficiency is a hallmark of Notch signaling across species—or even to a dominant-negative behavior. How, and indeed whether, a chronic exposure to reduced Notch signals leads to vSMC degeneration remains to be established. The proteomic profiling of human CADASIL postmortem brain vessels, the protein expression experiments in mice with CADASIL mutations

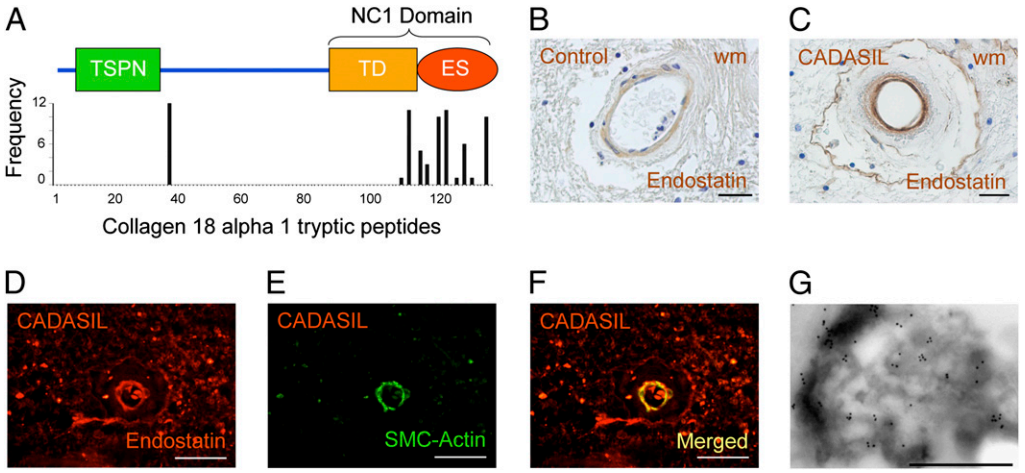

Fig. 5. Analysis of COL18A1/endostatin expression in cerebral vessels from individuals with CADASIL. (*A*) Schematic representation of COL18A1, isoform 2 (long; also see ref. 31). The N-terminal thrombospondin-like domain (TSPN) and the noncollagenous domain 1 (NC1) comprising the trimerization domain (TD) and the C-terminal endostatin domain (ES) are indicated. The graph shows the frequency of peptides along the length of COL18A1 detected by mass spectroscopy of arterial rings microdissected from postmortem brain sections of two individuals with the R1031C mutation. (*B* and *C*) Immunohistochemistry (IHC) with COL18A1/endostatin-specific antibodies shows abnormal distribution of this protein in the white matter (wm) of an individual carrying the R133C mutation (*C*) compared with control (*B*). (*D–F*) COL18A1/endostatin localizes primarily to the smooth muscle cell layer, labeled with α-actin (SMC-actin) in brain tissue from a R133C carrier. (*G*) Brain tissue from an individual with the R1031C (*G*) mutation was processed for immunogold labeling with an antibody against COL18A1/endostatin, which associates with GOMs. (Scale bars: *B* and *C*, 25 μm; D–*F*, 50 μm; *G*, 1 μm.)

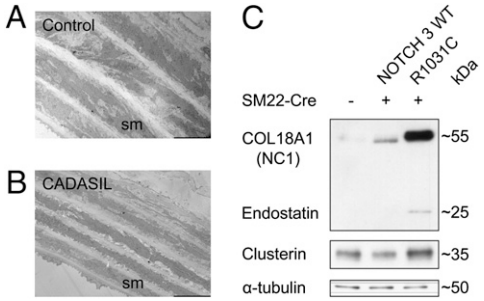

Fig. 6. Clusterin and COL18A1/endostatin are misregulated in transgenic mice expressing mutant Notch 3 receptors. (*A* and *B*) EM images of aortas from 12- to 14-mo-old animals expressing the R1031C mutation (*B*) show thinner layers of vSMCs compared with controls (*A*). (*C*) Western blot analysis of aortic protein extracts derived from 18-mo-old mice expressing WT Notch 3 or the R1031C mutation shows increased levels of clusterin (~35 kDa) and endostatin (~25 kDa) in mice expressing the mutant receptor. The endostatin antibody used for immunoblotting recognizes endostatin whether free (cleaved from COL18A1) or part of the COL18A1 molecule. The expression of an approximately 55-kDa protein, likely corresponding to the NC1 domain of COL18A1, is also significantly increased in the aorta of mutant animals compared with controls.

described here, as well as the RNA transcription profiling of brain-derived vSMCs from *Notch 3* KO mice described earlier (16), all point to an altered gene expression pattern as a consequence of loss of Notch function. Thus, loss of Notch 3 function may plausibly cause mutant phenotypes linked to stroke.

It is essential to point out that the evidence we gathered certainly does not exclude the possibility that CADASIL mutations, notwithstanding a hypomorphic nature, could also have neomorphic properties. Such properties may underlie, for instance, GOM formation. The causal relationship of the characteristic GOM deposits with the manifestation of CADASIL remains tenuous, but the proteomic analysis and the mouse models we developed provide important clues that may help elucidate this relationship. Keeping in mind the caveats discussed earlier regarding the equivalence of the osmiophilic deposits we document in mice with human GOMs, the existence of these deposits in transgenic mice expressing the CADASIL mutations is noteworthy. Moreover their age-dependent appearance in mice expressing the weak R1031C allele, in conjunction with the age-dependent manifestation of a hemodynamic phenotype, is particularly interesting as it parallels the degenerative nature of the disease. This, in turn, begets questions regarding a causal connection between the appearance of GOMs and stroke manifestation in CADASIL. If such a relationship exists, the apparent accumulation of clusterin and COL18A1/endostatin in arterial walls and GOMs may also be directly linked to CADASIL vessel pathology. Although such functional relationships would be difficult to establish in humans, our models offer the opportunity to explore this possibility.

Similar to all other models overexpressing CADASIL transgenes (24, 29, 30), our mice did not develop spontaneous strokes despite showing the pathological hallmarks of the disease, whereas the reported knock-in model showed no relevant phenotype (42). It is possible that the lack of strokes in the animal models may simply reflect species-specific characteristics of the cerebrovasculature and/or differences in lifespan that impose inherent limitations for the study of late-onset degenerative conditions like CADASIL. Nevertheless, we find the degree of similarity between individuals with CADASIL and our two mouse models remarkable. We also note that, although our mouse models can be compared with each other because each expresses the transgene at similar levels, it is difficult to compare them with other models, which express different levels of mutant and WT Notch receptors, notwithstanding differing genetic backgrounds.

The approach we used here, combining the analysis of patient-derived tissue with the generation of animal models and physiologic as well as biochemical functional assays, has proven to be informative. Given the sensitivity of development to Notch signal dosage and the extraordinary pleiotropy of Notch signaling, we believe that only such coordinated analysis has the potential to provide solid functional hints regarding the involvement of the Notch pathway in the vascular pathobiology associated with CADASIL and, more broadly, a possible involvement of Notch in ischemic stroke susceptibility. The link we uncovered among COL18A1/endostatin accumulation, Notch 3 mutations, and GOMs raises the interesting possibility that antiangiogenic mechanisms mediated by endostatin could play a role in CADASIL pathophysiology, which after all is the most prevalent monogenic cause of stroke and vascular dementia (8). It is possible that the models we generated for the study of Notch signaling in the vasculature may, beyond the study of CADASIL, provide more general insights into the biology of stroke and vascular dementia.

Materials and Methods

Mice. Animal care and experimental procedures were performed with approval from institutional animal care and use committees of Massachusetts General Hospital, Harvard Medical School, and Yale University. Littermates were used for comparative analysis throughout.

Human Subjects. Experiments involving postmortem human tissue were approved by the Massachusetts General Hospital Institutional Review Board.

Generation of Transgenic Mice. Mice conditionally expressing the *NOTCH* 3^{R1031C} and *NOTCH* 3^{C455R} transgenes from the ROSA26 (43) locus were generated as previously described (16). Primers were used to introduce the C455R or the R1031C mutations in the human *NOTCH 3* cDNA using multi-site-directed mutagenesis (Stratagene). The *NOTCH 3* coding region in both clones was fully sequenced after mutagenesis using sequencing primers before subcloning. Mutagenesis primers were as follows: C455R (GCATAGGCCAGTTCACCCGTATCTGTATGGCAGGC) and R1031C (CCTGGATGGAGCGGATGCCTCTGTGACATCC). The three strains have been deposited to the Jackson Laboratory and were named according to the guidelines of the International Committee on Standardized Genetic Nomenclature for Mice, MMRRC:032998 B6;129-*Gt*(*ROSA*)*26Sor*$^{tm1(NOTCH3)Sat}$/Mmjax; MMRRC:032999 B6;129-*Gt*(*ROSA*)*26Sor*$^{tm1(NOTCH3*R1031C)Sat}$/Mmjax; MMRRC:033000 129-*Gt*(*ROSA*)*26Sor*$^{tm2(NOTCH3*C455R)Sat}$/Mmjax. To generate mice expressing Dll1, the mouse Dll1 cDNA was amplified by PCR, sequenced and cloned directly into a targeting vector specific for the ROSA26 locus. In the final construct, Dll1 was flanked by a "loxed" stop cassette at the 5′ end and a polyadenylation sequence at the 3′ end. This construct was electroporated into ES cells (C57BL/6 NTac), followed by selection of positive lines by Southern blot hybridization. Chimeras generated through embryo injections of ES cells were crossed to BALB/c animals to obtain F1 mice.

Mouse Model of Focal Cerebral Ischemia. Experiments were performed as previously described (16). In brief, mice were anesthetized with isoflurane (2.5% induction, 1.5% maintenance, in 70% N_2O/30% O_2) and subjected to 1-h transient MCA occlusion using an intraluminal filament inserted via the external carotid artery. Regional cerebral blood flow was monitored using a laser Doppler probe placed over the core MCA territory. At 1-h occlusion, the filament was completely withdrawn to allow reperfusion. Infarct volume was calculated on TTC-stained 1-mm-thick coronal sections by the summation of the infarct areas in each of 10 brain sections, with the indirect method used to correct for edema (16). Eleven *NOTCH* 3^{WT}, eleven *NOTCH* 3^{WT};SM22-Cre (44), five *NOTCH* 3^{R1031C}, ten *NOTCH* 3^{R1031C};SM22-Cre, seven *NOTCH* 3^{C455R}, and seven *NOTCH* 3^{C455R};SM22-Cre mice were included in the analysis at the 3- to 6-mo-old time point. Thirteen *NOTCH* 3^{R1031C} and ten *NOTCH* 3^{R1031C};SM22-Cre mice were included in the analysis at the 1-y-old time point. All animals at both time points were in the *Notch 3* KO background. Data points were plotted by using Prism 5 for MacOSX (GraphPad). One-way ANOVA was used for analysis of values between groups. $P < 0.05$ was considered statistically significant.

Cell Culture. Primary MEFs were isolated following standard procedures from embryos at embryonic day 12.5. MEFs were cultured in Glasgow minimum essential medium, supplemented with 10% FBS, 2 mM L-glutamine, 100 μM

nonessential amino acids, 1 mM sodium pyruvate, 50 mM 2-mercaptoethanol, penicillin/streptomycin (50 U/mL and 50 μg/mL respectively), and 2.5 μg/mL Fungizone. All cell culture reagents were purchased from Gibco/Invitrogen. Early-passage (<5) cultures were used.

Adenovirus Infection. Adenovirus encoding the Cre recombinase (adeno-Cre) was purchased from the University of Iowa Gene Transfer Core. Twenty-four hours before infection, MEFs were plated at a density of 50,000 cells/cm^2. Transduction was performed at a multiplicity of infection of 500 pfu/cell for 3 h at 37 °C in minimal volume of culture medium diluted to 2% FBS. After infection, cells were rinsed in PBS solution and cultured in supplemented Glasgow minimum essential medium for 48 h. Efficiency of adeno-Cre–induced Cre/loxP recombination in MEFs was optimized in our laboratory by dosage of the Neomycin resistance (Neo) gene present in the STOP cassette. Briefly, DNA was extracted from fibroblasts 72 h after adeno-Cre infection, and amplification of the Neo gene was carried out in duplex with the amplification of the Ngf gene by using TaqMan technology (Applied Biosystems). The recombination efficiency was calculated as the ratio of Neo/Ngf by using a standard curve generated with WT MEFs or MEFs harboring one or two Neo cassettes. Infection at 500 pfu/cell gave more than 90% recombination efficiency 72 h after adeno-Cre infection in vitro. Primers, TaqMan probes, and protocols are available on the Jackson Laboratory Web site (www.jax.org).

Coculture Experiments. Forty-eight hours after receptor or ligand expression was induced by adeno-Cre–mediated recombination in vitro, cells were trypsinized and counted. Cocultures were performed at a 40%/60% ratio of receptor/ligand-expressing cells. As a control, Notch 3-expressing cells were cocultured at the same density with MEFs that had not been induced for Dll1 expression. Forty-eight hours after coculture, Notch 3-expressing cells, which also express EGFP, were isolated by FACS and directly lysed into RLT RNA extraction buffer (Qiagen). RNA was isolated using the RNeasy extraction kit with in-column DNase I digestion (Qiagen). Total RNA (600 ng) was used for reverse transcription using the High Capacity RNA-to-cDNA kit (Applied Biosystems). cDNA was diluted to 2 ng/mL equivalent RNA, and 6 ng equivalent RNA was used as template for qPCR by using TaqMan technology (Applied Biosystems) following the manufacturer's protocols. TATA box binding protein (Tbp) was used as internal control to normalize input. Data were processed with the $2^{-\Delta\Delta Ct}$ method (45). Fold change was calculated as the ratio of $2^{-\Delta\Delta Ct}$ (Notch 3-expressing MEFs cocultured with Dll1-expressing MEFs) to the average of $2^{-\Delta\Delta Ct}$ (Notch 3-expressing MEFs cocultured with WT MEFs). The following TaqMan gene expression assays (Applied Biosystems) were used: *Tbp* (Mm00446973_m1), *Heyl* (Mm00516555_m1), and *Hey1* (Mm00468865_m1). Data were analyzed and plotted using PRISM 5. One-way ANOVA followed by Tukey multiple comparison test were used for analysis of values between groups. *P* values lower than 0.05 were considered statistically significant.

LCM of Brain Vessels. Fifteen-micrometer sections were obtained from frozen blocks of subcortical white matter deriving from postmortem human tissue and stored at −80 °C until further processing. Slides were warmed to room temperature for 1 min under a hood and treated with 75% ethanol (denatured with 5% methanol and 5% isopropanol) for 1 min. Tissue sections were rehydrated in water for 1 min before staining, for 1 min, with Histogene staining solution (KIT0415; Arcturus). Sections were then washed in water for 1 min and dehydrated in increasing series of ethanol followed by xylene for 5 min. Finally, slides were air-dried in a low-humidity room before laser capture. Fifty arterioles were captured (46) per collecting cap (CapSure Macro LCM Caps; LCM0211; Arcturus) and stored in 0.5-mL tubes at −80 °C.

ACKNOWLEDGMENTS. We thank the Colombian and Finnish families with cerebral autosomal-dominant arteriopathy with subcortical infarcts and leukoencephalopathy for inspiring this work. We thank Katia Georgopoulos, Lin Wu, Jeffrey Wu, and the Massachusetts General Hospital transgenic mouse core facility for assistance in the generation of transgenic mice; Rachel E. Diamond of the Harvard NeuroDiscovery Center's Advance Tissue Research Center for help with laser capture microdissection; Suzan Lazo-Kallanian of the Hematologic Neoplasia Flow Cytometry Facility at Dana Farber Cancer Institute for help with the Notch signaling in vitro assay; Christoph Rahner and Morven Graham at the Center for Cell and Molecular Imaging at Yale School of Medicine for assistance with electron microscopy; and Glenn Doughty for help with animal husbandry. The Notch 3 mouse models generated for this study are available to the scientific community from the Jackson Laboratory under the auspices of the Mutant Mouse Regional Resource Centers program and National Institutes of Health (NIH). The mouse conditionally expressing Dll1 from the ROSA26 locus was generated in a collaboration between S.A.-T. and Dr. Jeffrey Greve at Exelixis. This work was supported by the Academy of Finland and the Sigrid Juselius Foundation (S.T.), the Migraine Pathophysiology and Treatment Mechanisms Program Project via NIH/National Institute of Neurological Disorders and Stroke Grant 5P01NS035611 (to M.A.M.), Yale School of Medicine (A.L.), and Sustainability Program 2010–2011 of the University of Antioquia (F.L.). Research in the S.A.-T. laboratory was supported by NIH Grants NS26084 and CA098402 and a gift from the Leduc family in Québec, Canada.

1. Thompson CS, Hakim AM (2009) Living beyond our physiological means: Small vessel disease of the brain is an expression of a systemic failure in arteriolar function: A unifying hypothesis. *Stroke* 40:e322–e330.
2. Joutel A, et al. (1996) Notch3 mutations in CADASIL, a hereditary adult-onset condition causing stroke and dementia. *Nature* 383:707–710.
3. Gould DB, et al. (2006) Role of COL4A1 in small-vessel disease and hemorrhagic stroke. *N Engl J Med* 354:1489–1496.
4. Revesz T, et al. (2003) Cerebral amyloid angiopathies: a pathologic, biochemical, and genetic view. *J Neuropathol Exp Neurol* 62:885–898.
5. Hara K, et al. (2009) Association of HTRA1 mutations and familial ischemic cerebral small-vessel disease. *N Engl J Med* 360:1729–1739.
6. Federico A, Bianchi S, Dotti MT (2005) The spectrum of mutations for CADASIL diagnosis. *Neurol Sci* 26:117–124.
7. Low WC, et al. (2007) Hereditary multi-infarct dementia of the Swedish type is a novel disorder different from NOTCH3 causing CADASIL. *Brain* 130:357–367.
8. Chabriat H, Joutel A, Dichgans M, Tournier-Lasserve E, Bousser MG (2009) Cadasil. *Lancet Neurol* 8:643–653.
9. Ruchoux MM, et al. (1995) Systemic vascular smooth muscle cell impairment in cerebral autosomal dominant arteriopathy with subcortical infarcts and leukoencephalopathy. *Acta Neuropathol* 89:500–512.
10. Tikka S, et al. (2009) Congruence between NOTCH3 mutations and GOM in 131 CADASIL patients. *Brain* 132:933–939.
11. Baudrimont M, Dubas F, Joutel A, Tournier-Lasserve E, Bousser MG (1993) Autosomal dominant leukoencephalopathy and subcortical ischemic stroke. A clinicopathological study. *Stroke* 24:122–125.
12. Brulin P, Godfraind C, Leteurtre E, Ruchoux MM (2002) Morphometric analysis of ultrastructural vascular changes in CADASIL: Analysis of 50 skin biopsy specimens and pathogenic implications. *Acta Neuropathol* 104:241–248.
13. Louvi A, Arboleda-Velasquez JF, Artavanis-Tsakonas S (2006) CADASIL: A critical look at a Notch disease. *Dev Neurosci* 28:5–12.
14. Domenga V, et al. (2004) Notch3 is required for arterial identity and maturation of vascular smooth muscle cells. *Genes Dev* 18:2730–2735.
15. Liu H, Zhang W, Kennard S, Caldwell RB, Lilly B (2010) Notch3 is critical for proper angiogenesis and mural cell investment. *Circ Res* 107:860–870.
16. Arboleda-Velasquez JF, et al. (2008) Linking Notch signaling to ischemic stroke. *Proc Natl Acad Sci USA* 105:4856–4861.
17. Artavanis-Tsakonas S, Rand MD, Lake RJ (1999) Notch signaling: Cell fate control and signal integration in development. *Science* 284:770–776.
18. Kopan R, Ilagan MX (2009) The canonical Notch signaling pathway: Unfolding the activation mechanism. *Cell* 137:216–233.
19. Joutel A, et al. (1997) Strong clustering and stereotyped nature of Notch3 mutations in CADASIL patients. *Lancet* 350:1511–1515.
20. Arboleda-Velasquez JF, et al. (2002) C455R notch3 mutation in a Colombian CADASIL kindred with early onset of stroke. *Neurology* 59:277–279.
21. Peters N, et al. (2004) CADASIL-associated Notch3 mutations have differential effects both on ligand binding and ligand-induced Notch3 receptor signaling through RBP-Jk. *Exp Cell Res* 299:454–464.
22. Karlström H, et al. (2002) A CADASIL-mutated Notch 3 receptor exhibits impaired intracellular trafficking and maturation but normal ligand-induced signaling. *Proc Natl Acad Sci USA* 99:17119–17124.
23. Low WC, Santa Y, Takahashi K, Tabira T, Kalaria RN (2006) CADASIL-causing mutations do not alter Notch3 receptor processing and activation. *Neuroreport* 17: 945–949.
24. Monet-Leprêtre M, et al. (2009) Distinct phenotypic and functional features of CADASIL mutations in the Notch3 ligand binding domain. *Brain* 132:1601–1612.
25. Haritunians T, et al. (2002) CADASIL Notch3 mutant proteins localize to the cell surface and bind ligand. *Circ Res* 90:506–508.
26. Hofmann JJ, Iruela-Arispe ML (2007) Notch signaling in blood vessels: Who is talking to whom about what? *Circ Res* 100:1556–1568.
27. Joutel A, et al. (2000) The ectodomain of the Notch3 receptor accumulates within the cerebrovasculature of CADASIL patients. *J Clin Invest* 105:597–605.
28. Brass SD, Smith EE, Arboleda-Velasquez JF, Copen WA, Frosch MP (2009) Case records of the Massachusetts General Hospital. Case 12-2009. A 46-year-old man with migraine, aphasia, and hemiparesis and similarly affected family members. *N Engl J Med* 360:1656–1665.
29. Ruchoux MM, et al. (2003) Transgenic mice expressing mutant Notch3 develop vascular alterations characteristic of cerebral autosomal dominant arteriopathy with subcortical infarcts and leukoencephalopathy. *Am J Pathol* 162:329–342.
30. Joutel A, et al. (2010) Cerebrovascular dysfunction and microcirculation rarefaction precede white matter lesions in a mouse genetic model of cerebral ischemic small vessel disease. *J Clin Invest* 120:433–445.

31. O'Reilly MS, et al. (1997) Endostatin: an endogenous inhibitor of angiogenesis and tumor growth. *Cell* 88:277–285.
32. Folkman J (2006) Antiangiogenesis in cancer therapy—endostatin and its mechanisms of action. *Exp Cell Res* 312:594–607.
33. Wilson MR, Easterbrook-Smith SB (2000) Clusterin is a secreted mammalian chaperone. *Trends Biochem Sci* 25:95–98.
34. Yerbury JJ, et al. (2007) The extracellular chaperone clusterin influences amyloid formation and toxicity by interacting with prefibrillar structures. *FASEB J* 21: 2312–2322.
35. Harold D, et al. (2009) Genome-wide association study identifies variants at CLU and PICALM associated with Alzheimer's disease. *Nat Genet* 41:1088–1093.
36. Lambert JC, et al; European Alzheimer's Disease Initiative Investigators (2009) Genome-wide association study identifies variants at CLU and CR1 associated with Alzheimer's disease. *Nat Genet* 41:1094–1099.
37. Wyatt A, Yerbury J, Poon S, Dabbs R, Wilson M (2009) Chapter 6: The chaperone action of Clusterin and its putative role in quality control of extracellular protein folding. *Adv Cancer Res* 104:89–114.
38. Ishiko A, et al. (2006) Notch3 ectodomain is a major component of granular osmiophilic material (GOM) in CADASIL. *Acta Neuropathol* 112:333–339.
39. Mykkänen K, et al. (2004) Detection of the founder effect in Finnish CADASIL families. *Eur J Hum Genet* 12:813–819.
40. Miao Q, et al. (2004) Fibrosis and stenosis of the long penetrating cerebral arteries: the cause of the white matter pathology in cerebral autosomal dominant arteriopathy with subcortical infarcts and leukoencephalopathy. *Brain Pathol* 14:358–364.
41. Santa Y, et al. (2003) Genetic, clinical and pathological studies of CADASIL in Japan: a partial contribution of Notch3 mutations and implications of smooth muscle cell degeneration for the pathogenesis. *J Neurol Sci* 212:79–84.
42. Lundkvist J, et al. (2005) Mice carrying a R142C Notch 3 knock-in mutation do not develop a CADASIL-like phenotype. *Genesis* 41:13–22.
43. Soriano P (1999) Generalized lacZ expression with the ROSA26 Cre reporter strain. *Nat Genet* 21:70–71.
44. Holtwick R, et al. (2002) Smooth muscle-selective deletion of guanylyl cyclase-A prevents the acute but not chronic effects of ANP on blood pressure. *Proc Natl Acad Sci USA* 99:7142–7147.
45. Livak KJ, Schmittgen TD (2001) Analysis of relative gene expression data using real-time quantitative PCR and the 2(-Delta Delta C(T)) method. *Methods* 25:402–408.
46. Emmert-Buck MR, et al. (1996) Laser capture microdissection. *Science* 274:998–1001.